JOURNAL OF
EMERGING INVESTIGATORS

Article

VISTA inhibitor CA170 combined with *KRAS* vaccine enhances immune response in lung cancer

Chloe Giglio[1], Ashley Pearson[2]
[1] McLean High School, McLean, Virginia
[2] Graduate Program in Immunology, University of Michigan, Ann Arbor, Michigan

SUMMARY

Lung cancer is the leading cause of cancer-related death globally. Immune checkpoint inhibitors (ICI) have emerged as a promising therapy for late-stage lung cancer. However, their response rate remains low, highlighting the need to explore diverse intervention pathways to optimize antitumor efficacy. CA170, a small molecule targeting immune checkpoints Programmed Cell Death Protein 1 (PD-1) and V-domain Ig Suppressor of T cell Activation (VISTA), is highly expressed in the lungs and offers an advantage over antibody-based ICIs due to its membrane permeability. We hypothesized that a combination therapy of CA170, an antigen-independent small molecule, and *KRAS* vaccine (Kvax), an antigen-specific vaccine targeting the Kirsten rat sarcoma viral oncogene homolog (*KRAS*) mutation in lung cancer, would promote antitumor immune response pathways more strongly than either treatment alone. To test this hypothesis, we analyzed publicly available single-cell RNA sequencing (scRNA-seq) data to examine the effects of the treatment on immune cell compartments. We evaluated immune cell response pathways identified through receptor-ligand analysis via CellChat. Our findings indicate that the combination therapy of CA170 and Kvax enhances helper T cell function and improves cytotoxic T lymphocyte infiltration, while Kvax alone drives plasma and memory B cell proliferation. This study suggests that combining antigen-specific vaccines and antigen-independent ICIs may enhance the antitumor response in lung cancer. Our findings could aid in developing more effective strategies to extend the efficacy of immunotherapy in lung cancer patients.

INTRODUCTION

Globally, lung cancer accounts for the highest proportion of cancer-related deaths, comprising nearly 18% of total cancer mortality (1). Each year, lung cancer mortalities surpass the combined deaths from colon, breast, and prostate cancers (2). The main types of lung cancer include small cell lung cancer and non-small cell lung cancer (NSCLC) which comprises around 87% of lung cancer cases (2). The 5-year survival rates in the United States are 9% for small cell and 32% for non-small cell lung cancers (3). For early stages of lung cancer, surgical treatment or radiation therapy improves survival outcomes (4). However, 47% of lung cancer diagnoses occur at a late stage, when these treatments become less effective and the survival rate is only 6% (5). For advanced metastatic lung cancer, chemotherapy, immunotherapy, and targeted therapies are more effective treatment options than surgical interventions and radiation therapy (6).

The tumor microenvironment (TME) plays a central role in determining how cancers progress and how they respond to therapy. The TME is a complex milieu of cancer cells, signaling molecules and infiltrating immune cells, including cytotoxic T lymphocytes (CTLs), helper T cells, and B cells (7). Helper T cells produce cytokines that activate other immune cells, such as CTLs (8, 9). CTLs recognize tumor antigens and directly kill cancer cells (8, 9). B cells produce tumor-specific antibodies, present antigens to T cells, and differentiate into antibody-producing plasma B cells or long-lived memory B cells that support long-term immune memory responses (8). For effective antitumor immunity, these cancer-fighting immune cells must infiltrate the tumor and become activated within the TME (7).

However, many tumors create an immunosuppressive TME that prevents these immune cells from functioning effectively. A major mechanism of immunosuppression is the engagement of immune checkpoints, which inhibit overactivation of the immune system and perpetuate tolerance to self (10). For example, immune checkpoint receptor programmed cell death protein 1 (PD-1) on T cells bind to ligand programmed death-ligand 1 (PD-L1), on an antigen-presenting cell, to dampen the severity of the immune response and minimize tissue damage (11). However, in an immunosuppressive TME, cancer cells can exploit these mechanisms by expressing checkpoint ligands to inhibit T cells and evade immune surveillance (10). Hence, immune checkpoint inhibitors (ICIs) were developed to block cancer cell interactions with inhibitory checkpoints, allowing the immune system to mount a more effective antitumor response (12, 13, 14). In recent decades, these therapies have become an important part of cancer treatment regimens and significantly improved clinical outcomes for lung cancer patients (12, 13). Current monoclonal antibody (mAb) ICIs that target PD-1/PD-L1 augment T cell infiltration into tumors and enhance progression-free survival in lung cancer patients (15, 16). Despite their promise, the efficacy of these mAb-based ICIs remains limited due to poor tissue permeability, resulting in response rates below 30% among NSCLC patients (17, 18). These limitations highlight the need for therapies that more effectively reach the tumor.

A promising approach is the combination of CA170, a small-molecule dual ICI, with a vaccine targeting the Kirsten rat sarcoma virus (KRAS) mutation. Small molecules, like CA170, offer advantages over mAb, including better tumor infiltration and the ability to target intracellular pathways inaccessible to antibodies (19). Additionally, CA170's short half-life lowers toxicity compared to mAb-based ICIs (20). CA170 targets two distinct immune checkpoints: PD-L1 and

https://doi.org/10.59720/24-358

V-domain immunoglobulin suppressor of T cell activation (VISTA). VISTA functions through pathways distinct from the PD-1/PD-L1 immune checkpoint. As both a ligand and receptor, VISTA can be expressed on antigen-presenting cells (APCs) or T cells to mediate inhibitory signals. These interactions suppress T cell activation, proliferation, and cytokine production (17, 21). VISTA makes lung tumors a good target for ICI therapy as it is expressed in around 99% of NSCLCs and is associated with increased tumor-infiltrating lymphocytes (22). However, like other ICIs, CA170 does not target a specific tumor antigen as VISTA is expressed on non-tumor cells (23, 24). This lack of specificity allows it to be applied across a broad range of cancers, but also increases the risk of off-tumor autoimmune damage (14).

Tumor specificity may be improved by pairing CA170 with Kvax, a multi-peptide vaccine designed to target the *KRAS* G12C mutation, one of the most common oncogenic drivers of lung adenocarcinoma (25, 26). As a proto-oncogene, the *KRAS* gene mutation promotes uncontrolled cell division and tumor growth and is often associated with poor prognosis and resistance to conventional therapies (25, 26). Kvax delivers mutated KRAS peptides to antigen-presenting cells, such as B cells, stimulating their proliferation and differentiation and enabling them to activate T cells which selectively recognize and kill mutated KRAS-presenting tumor cells (27, 28). By directing immune activation toward a tumor-specific neoantigen, Kvax may help focus the broader CA170-induced immune response on KRAS-mutant tumor cells, potentially improving tumor specificity and reducing off-tumor effects (23, 27).

While considerable research has explored the antitumor efficacy of CA170, the combination effects of CA170 and Kvax have been examined only once. In that study, flow cytometry and a single-cell RNA-sequencing (scRNA-seq) analysis revealed that a combination of CA170 and Kvax increased T cell infiltration, an expansion of helper T cells, and reduced tumor load and multiplicity in a lung cancer mouse model (23). While the previous study primarily focused on *in vivo* findings, our research expands on this study by providing a detailed examination of the expression of cellular signaling pathways and transcriptional signatures associated with differentiation, proliferation, functionality, and migration in specific T cell subtypes. Additionally, the role of B cells in response to VISTA ICIs remains largely unexplored in the literature. Our study provides a novel examination of B-cell activity in the lung TME, offering new insights into their potential role in immunotherapy.

We hypothesized that a combination therapy of ICI CA170 and antigen-specific Kvax would promote transcriptional programs associated with antitumor immune response pathways more strongly than either treatment alone. To test our hypothesis, we conducted a new analysis on publicly available scRNA-seq data of immune cells from murine lung cancer samples. Our study revealed an expansion of helper T cell proportion and function, enhanced T cell migration, and increased memory B cell and plasma cell proliferation, despite a decrease in follicular B cell proliferation in the treatment groups compared to the control. By highlighting the enhanced effects of CA170 and Kvax combination therapy on both T and B cell populations in the lung TME, our findings provide a comprehensive examination of the T cell antitumor response and introduce novel insights into B cell antitumor pathways. This deeper understanding of how CA170 and Kvax influence immune responses in lung cancer could inform future immunotherapeutic strategies.

RESULTS

Assessment of the Changes in Immune Cell Compartments across all Treatment Groups

The lung cancer TME holds essential information to understand responses to immunotherapy (29). To determine which immune cells were driving the antitumor responses, we analyzed how each treatment group affected the proportion of immune cells in the TME. We downloaded a murine lung cancer dataset from the Gene Expression Omnibus (GEO). The dataset consisted of 20 samples collected by Pan et al. from five to six-week-old female mice with carcinogen-induced primary lung tumors and sequenced using scRNA-seq (23, 30). We performed scRNA-seq analysis in R (version 4.4.0) using Seurat (version 5.1.0) (31, 32). Our analysis focused on immune cells in lung tumors across five treatment groups: control (PBS), adjuvant control (STING agonist), CA170, Kvax with adjuvant, combo treatment group of CA170, Kvax, and adjuvant. STING agonists promote inflammation in the TME and enhance lymphocyte activity through the production of cytokines, such as TNF-α and IL-6 (33). For this reason, several STING agonists have shown clinical promise in improving immunotherapy efficacy (33). In the Kvax and combination groups, STING agonists were included to assess a clinically relevant immune response with Kvax. They were also included as a control to account for inflammatory effects. Based on common gene markers, we identified distinct immune cell clusters for dendritic cells, natural killer cells (NK), myeloid cells, T cells, and B cells **(Figure 1)**. Then, we calculated their proportion distributions across the five different treatment groups **(Figure 2).** Notably, B and T cells comprised over half of the total immune cell population in all groups, and B and T cell proportions differed significantly between the control and combo treatment groups, the control and CA170 groups, and the control and Kvax groups (chi-squared test; $p < 0.0001$ for all three comparisons) **(Figures 2A, B)**. B cells decreased more than two-fold, from 38.58% in the control to 18.11% in the combo treatment group, while T cells nearly doubled, increasing from 26.02% in the adjuvant group to 44.62% in the combo treatment group **(Figure 2A)**. In contrast, myeloid cells increased by around 40%, and NK cells were reduced by almost 20% (**Figure 2A)**. Based on these findings, we hypothesized that alterations in B and T cells were the primary drivers of the antitumor response.

Additionally, significant changes in the proportion of T cell subtypes were observed in the combo treatment group. We identified both $CD4^+$ and $CD8^+$ CTL groups, so the term "CTL" refers to both $CD4^+$ and $CD8^+$ CTLs (**Figure 2C**). We also identified $CD8^+/CD4^+$ memory effector cells, $CD8^+$ naïve cells, $CD8^+/CD4^+$ naïve cells, and $CD4^+$ helper T cells (**Figure 2C**). We observed a remodeling of the helper T cell and CTL compartments in the Kvax and combo treatment groups compared to the control group (chi-squared test; $p < 0.0001$; $p < 0.0001$, $p < 0.0001$; $p < 0.0001$) **(Figures 2C, D)**. The proportion of helper T cells notably expanded in the Kvax and

https://doi.org/10.59720/24-358

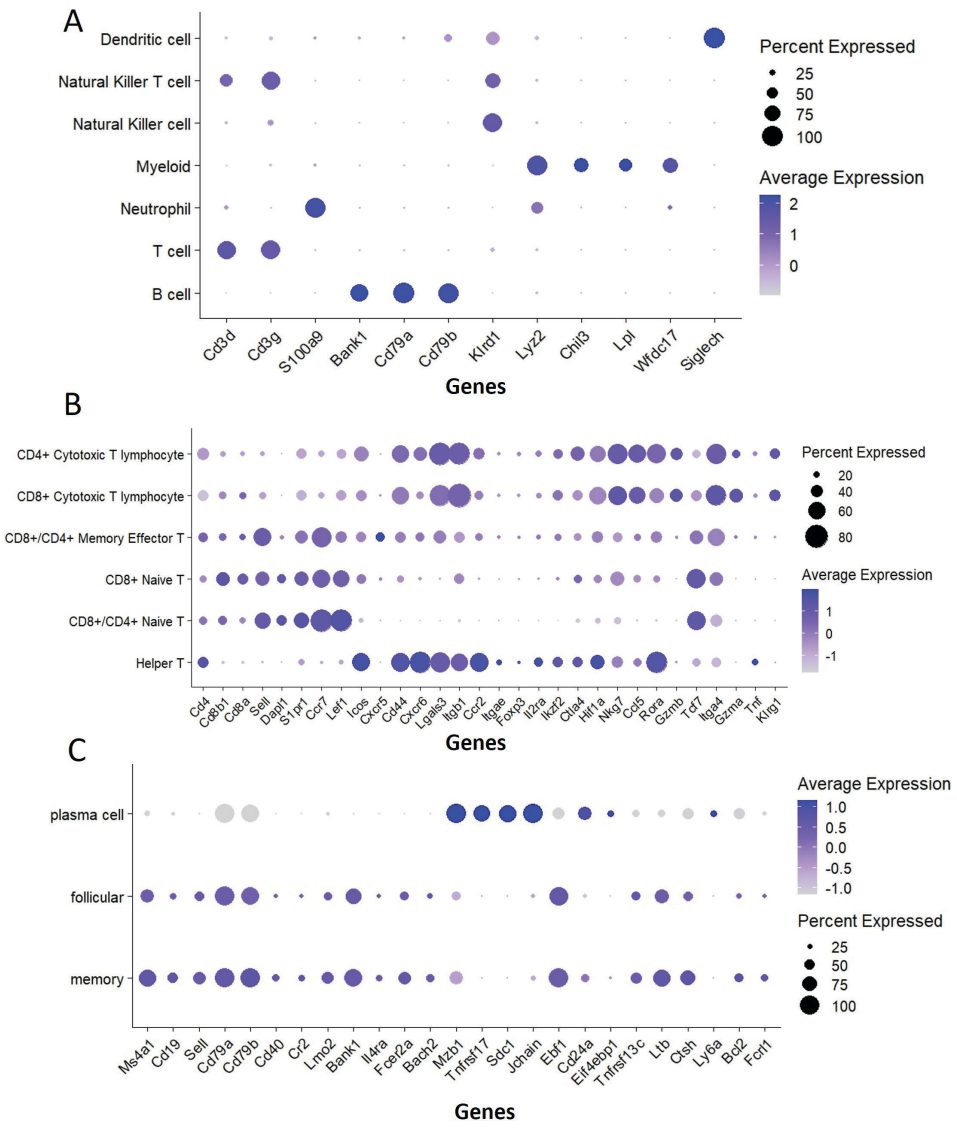

Figure 1: B and T cell subtypes were identified based on gene signatures. (A) Marker gene expression for each cell type, where dot size and color represent the percentage of marker gene expression and the averaged scaled expression value, respectively. (B) Marker gene expression for each T cell type. (C) Marker gene expression for each B cell type.

combo treatment groups compared to the control, increasing from 32.29% in the control to 64.55% in the Kvax and 57.63% in the combo treatment groups, respectively **(Figure 2D)**. Meanwhile, naïve T cell proportions decreased from 56.50% in the control to 27.32% in the Kvax and 27.32% in the combo treatment groups.

Regarding B cell subtypes, memory, follicular, and plasma B cells were identified. The Kvax and combo treatment groups exhibited significant alterations across all subtype compartments when compared to the control group (chi-squared test; $p < 0.0001$ for all comparisons) **(Figures 2E, F)**. The Kvax and combo treatments induced expansions and suppressions of B and T cell subtypes, indicating a potential shift in the immune response dynamics within the TME.

Furthermore, we analyzed gene expressions of common gene markers for each cell subtype across treatment groups **(Figure 3)**. The marker gene expression patterns of naïve T cells, helper T cells, all CTLs, and memory B cells were consistent with the observed changes in cell type proportions, indicating shifts in cellular activation states **(Figures 2D, E, 3A-D)**. Interestingly, while the proportion of memory effector T cells decreased in the CA170 and combo treatment groups, their marker gene expression levels were substantially higher in those groups **(Figures 2D, 3D)**. This suggests that the observed decrease in memory effector T cell proportion was likely due to an expansion of other immune cell proportions rather than a reduction in memory effector T cell activity. Additionally, although the proportions of follicular B cells and plasma B cells increased in the combo treatment group compared to the control, their marker gene expression levels were most pronounced in the control group **(Figures 2E, 3E, 3F)**. This discrepancy highlights the need for further

https://doi.org/10.59720/24-358

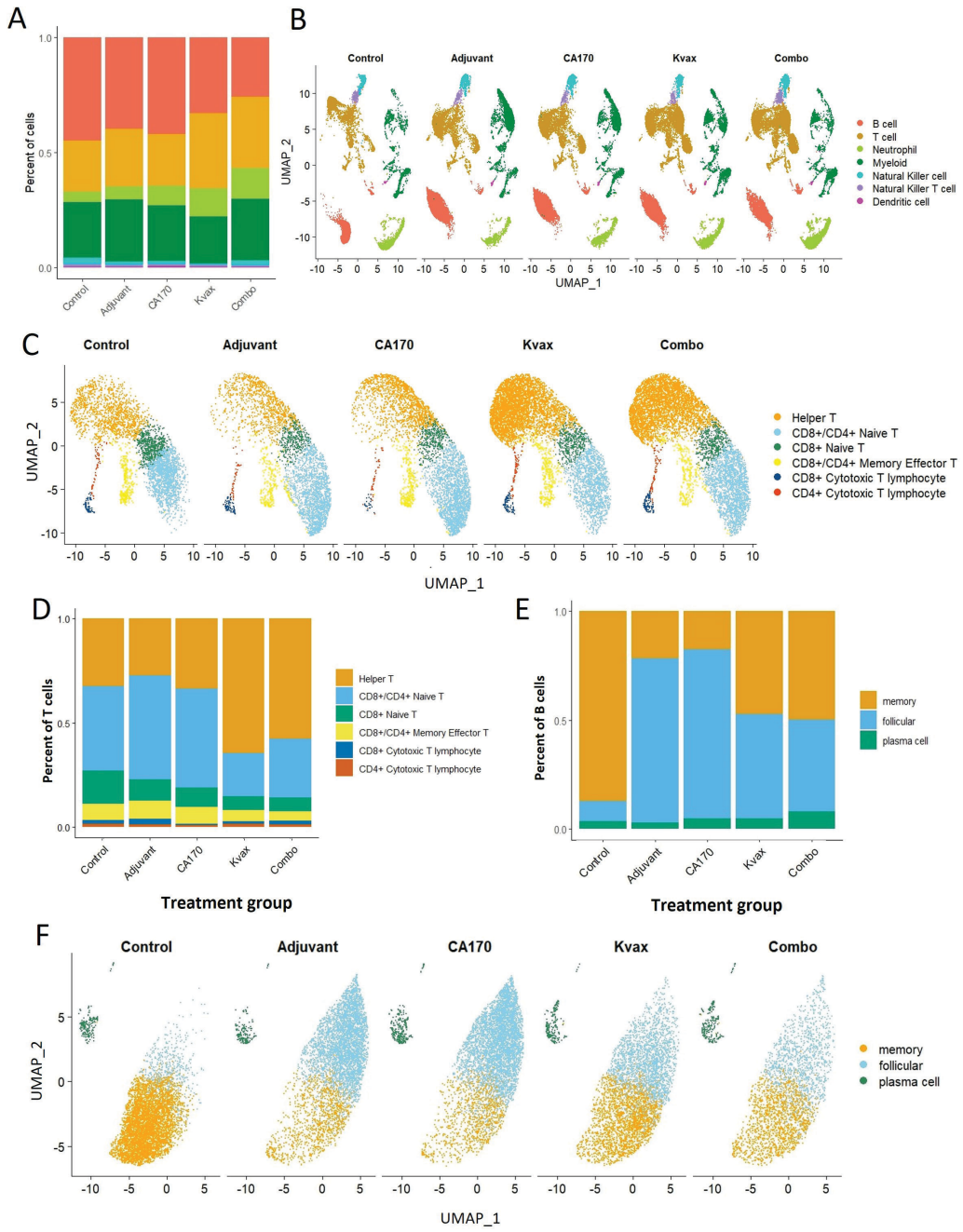

Figure 2: The treatment groups affect the proportion of immune cells. (A) Proportions of cell types (B cell, T cell, neutrophil, myeloid, natural killer cell, natural killer T cell, dendritic cell) across all treatment groups. The dendrogram was clustered by hierarchical clustering. (B) Labeled Uniform Manifold Approximation and Projection (UMAP) projection showing cellular heterogeneity differentiated by treatment group. (C) Sub-clustered T cells differentiated by treatment group. (D) Proportion of different T cells for the five treatment groups. (E) Proportion of different B cells for the five treatment groups. (F) Sub-clustered B cells differentiated by treatment group.

investigation into the functional roles of follicular and plasma B cells in the context of immune checkpoint inhibitors and cancer vaccines.

Identification of Highly Expressed Immune Cell Pathways

To determine the specific pathways and cell types that were driving changes in B and T cell proportions, we performed receptor-ligand analysis via CellChat, a tool that quantitatively infers active cellular pathways and communication networks in scRNA-seq data based on receptor-ligand interactions (34). The analysis revealed stronger outgoing interactions from B and T cells compared to the other CD45^{+} cells, suggesting that B and T cells are actively influencing the behavior of other immune cells via cell-to-cell interactions **(Figure 4A)**. We then visualized the relative expression of the top 20 receptors and ligands across all treatment groups **(Figures 4B, C)**. The

https://doi.org/10.59720/24-358

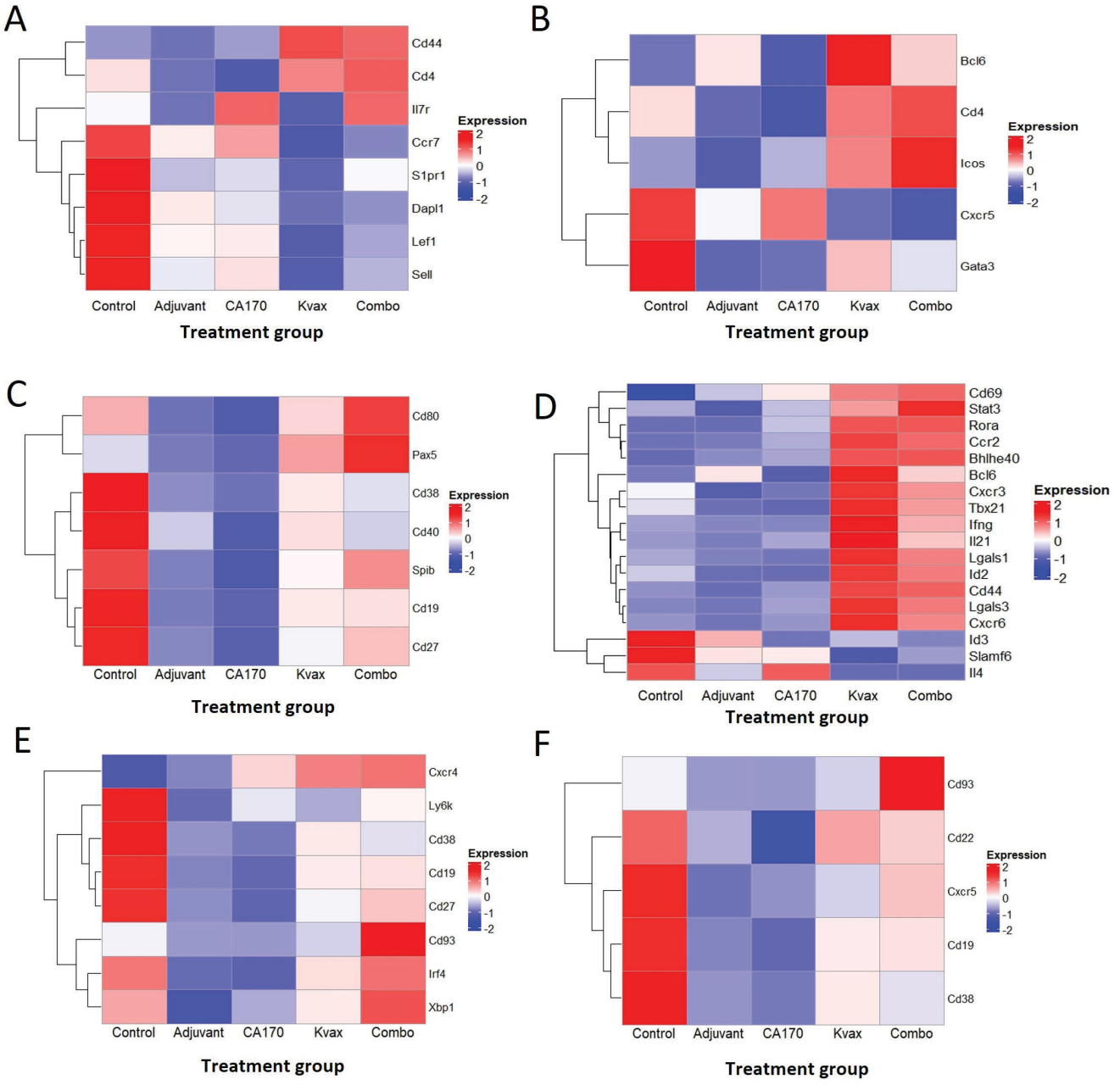

Figure 3: Marker gene expressions for each cell subtype are compared across treatment groups. For each of the seven T and B cell subtypes (naïve T cell, memory effector T cell, helper T cell, cytotoxic T cell (CTL), plasma B cell, memory B cell, follicular B cell), gene expression for common murine gene markers was averaged into heatmaps. The dendrograms were clustered by hierarchical clustering. (A) Naïve T cell gene markers tested within T cells. (B) Helper T cell gene markers tested within T cells. (C) Memory B cell gene markers tested within B cells. (D) Memory effector T cell gene markers tested within T cells. (E) Plasma B cell gene markers tested within B cells. (F) Follicular B cell gene markers tested within B cells.

combo treatment group exhibited elevated expressions of *Cd44*, *Cxcr4*, *Ccr1*, *Ccr5*, and *Ccr7*, genes associated with the regulation of immune cell adhesion and migration **(Figure 3B)** (35-37). This finding suggests that CA170 combined with Kvax promotes immune cell migration and tumor infiltration. Most of the top ligand genes were dominated by major histocompatibility complexes (MHCs) such as H2-Q6 and H2-K1, indicating communications between T cells and antigen-presenting cells **(Figure 4C)** (38-40). Notably, these interactions were more highly expressed in the control group compared to other treatment groups, suggesting more antigen-presentation interactions in the control group **(Figure 4C)**.

https://doi.org/10.59720/24-358

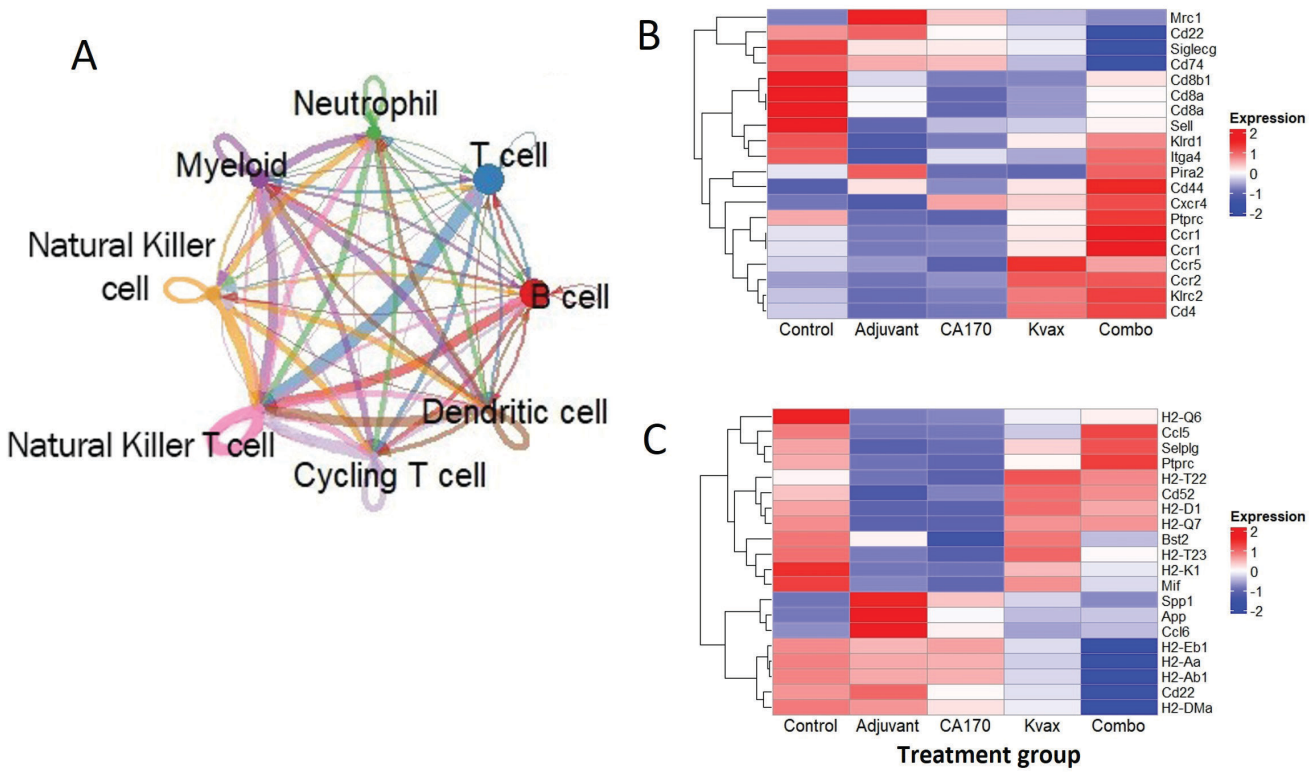

Figure 4: T cell activation, antigen presentation, and immune cell migration are key upregulated pathways. CellChat was run on the CD45⁺ object to identify the main interactions between cell types and infer the top receptor-ligand pairs. (A) Interaction network showing the strengths of outgoing and incoming signals between each cell type in the CD45⁺ object. The arrows point from the cell containing the ligand to the cell containing the receptor. Wider arrows indicate stronger interactions, and each color corresponds to the cell producing the outgoing signal. (B) Top 20 significant receptor genes analyzed on the entire CD45⁺ object. (C) Top 20 significant ligand genes analyzed on the CD45⁺ object. The dendrogram was clustered by hierarchical clustering.

Effect of CA170/Kvax Combination Treatment on Helper T Cell Activity

Given the notable increase in helper T cell proportion in the Kvax and combo treatment groups compared to the control, we hypothesized that the combo treatment group would enhance helper T cell function. To test this, we analyzed gene pathways from the Gene Ontology (GO) database related to helper T cell differentiation, immune response, and cytokine production (41). We then calculated the average gene expression in each pathway and compared the results across treatment groups.

Pathway analysis revealed significantly higher gene expression of helper T cell differentiation markers in the CA170 and Kvax treatment groups compared to the control (two-way ANOVA with Tukey HSD, $p < 0.0001$, $p < 0.0001$, respectively) **(Figure 5A)**. Importantly, there was also a significant interaction between CA170 and Kvax in promoting gene expression programs associated with helper T cell differentiation (two-way ANOVA; $p < 0.0001$), indicating that the effect of one treatment condition depended on the presence or absence of the other. Post-hoc Tukey HSD analysis (HSD = 0.01) revealed that pairwise differences between cell means were statistically significant **(Figure 5A)**. These findings confirmed the observed expansion of helper T cell proportion. To assess helper T cell function, we analyzed immune response and cytokine production, key indicators of helper T cell activity. According to the GO database, immune response is defined as any process that increases the frequency, extent, or rate of helper T cell activity. We observed a significant increase in helper T cell immune response and cytokine production in the CA170 and Kvax treatment groups compared to the control (two-way ANOVA with Tukey HSD, $p < 0.0001$; $p < 0.0001$, respectively), along with a strong interaction between CA170 and Kvax (two-way ANOVA with Tukey HSD, $p < 0.01$) **(Figure 5B-D)**. These findings suggest that while CA170 and Kvax individually promote helper T cell expansion and function, their combination further enhances helper T cell activity, ultimately strengthening the antitumor immune response.

Assessment of CTL Migration and Infiltration

Our CellChat analysis revealed a strong expression of pathways associated with immune cell migration and infiltration **(Figure 4B)**. Given the importance of T cell infiltration for an effective antitumor response, we examined whether the combo treatment enhanced T cell migration and tumor infiltration by analyzing T cell chemotaxis, the movement of T cells toward tumors in response to chemical signals, and extravasation, the diffusion of T cells from the bloodstream into surrounding tissues (42, 43). Using the GO

https://doi.org/10.59720/24-358

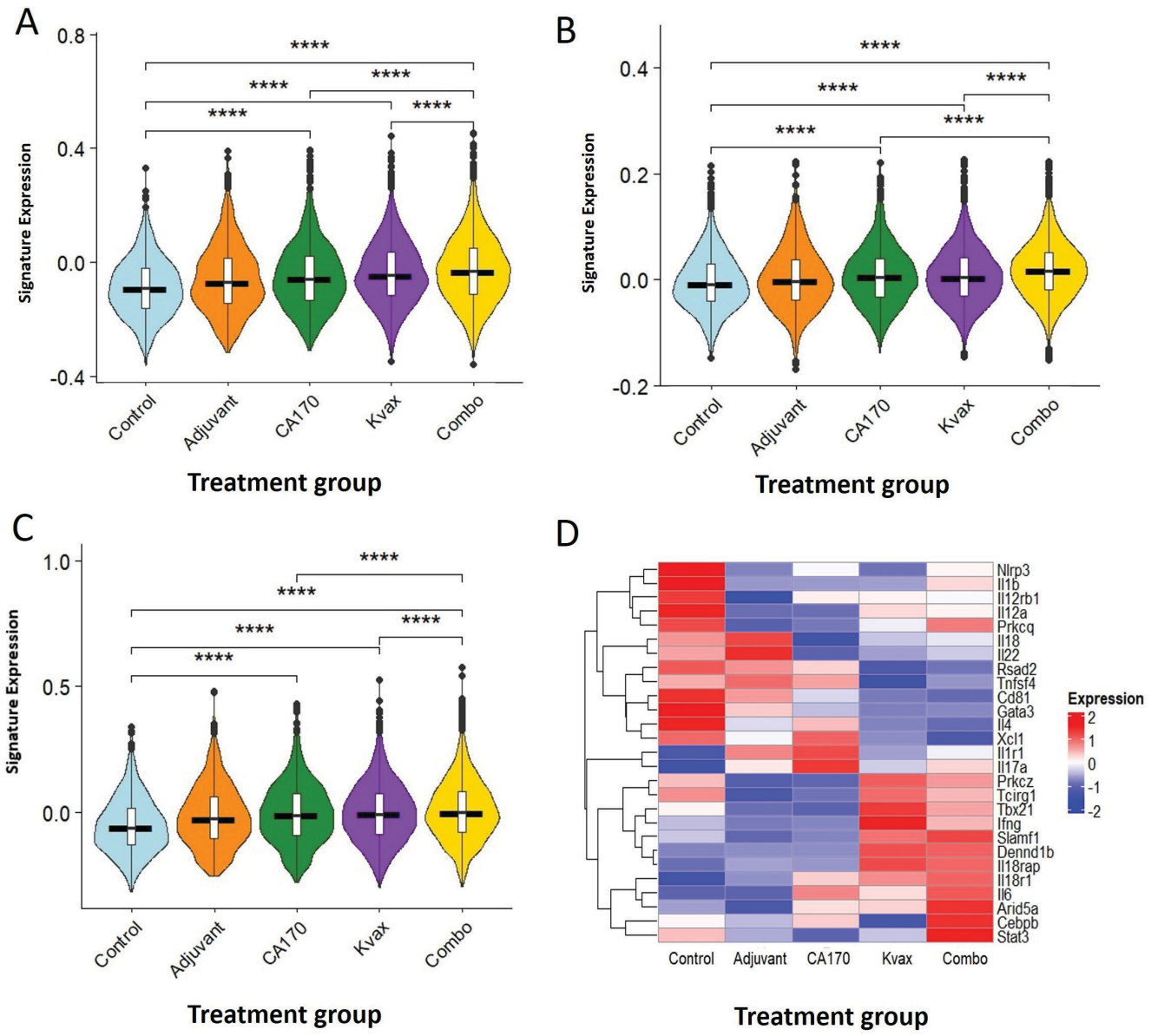

Figure 5: The CA170/Kvax combo treatment induces helper T cell differentiation and activity. Gene signatures for helper T cell differentiation and activation were obtained from the GO database, and the average signature expression for each treatment group was calculated. The black lines on the violin plots represent median gene expression values. (A) Average helper T cell differentiation gene expression analyzed on T cells. The median values, rounded to the thousandths place for each of the five treatment groups from left to right, are as follows: control was -0.093, adjuvant was -0.071, CA170 was -0.059, KRAS vaccine (Kvax) was -0.047, combo was -0.032. CA170 and Kvax had a significant difference on mean gene expression levels compared to the control group (two-way ANOVA with Tukey HSD, $p < 0.0001$). There was a significant interaction between CA170 and Kvax in influencing mean gene expression levels *(*two-way ANOVA with Tukey HSD, $p < 0.0001$). (B) Average helper T cell immune response gene expression analyzed on helper T cells. Median values: -0.009, -0.003, 0.005, 0.004, 0.017. CA170 and Kvax had a significant difference on mean gene expression levels compared to the control (two-way ANOVA with Tukey HSD, $p < 0.0001$). The interaction between CA170 and Kvax was significant *(*two-way ANOVA with Tukey HSD, $p = 0.0011$). (C) Average helper T cell cytokine production gene expression analyzed on helper T cells. Median values: -0.063, -0.026, -0.011, -0.008, -0.002. CA170 and Kvax had a significant difference on mean gene expression levels compared to the control (two-way ANOVA with Tukey HSD, $p < 0.0001$). The interaction between CA170 and Kvax was significant *(*two-way ANOVA with Tukey HSD, $p < 0.0001$). (D) Heatmap showing average expression of helper T cell immune response genes and helper T cell cytokine production genes analyzed on helper T cells. The dendrogram was clustered by hierarchical clustering. Two-way ANOVAs and Tukey post-hoc tests were performed on each pathway to examine the main effects of CA170 and Kvax and their interaction, **** $p < 0.0001$.

https://doi.org/10.59720/24-358

Signature	GO Source Number	Literature
T cell		Hu et al. (66)
B cell		Hu et al. (66)
Neutrophil		Hu et al. (66)
Myeloid		Hu et al. (66)
NK		Hu et al. (66)
NKT		Hu et al. (66)
Dendritic		Hu et al. (66)
Helper T		Pan et al. (19)
Naïve T		Pan et al. (19)
Memory effector T		Pan et al. (19)
CTL		Pan et al. (19)
Memory B		(68)
Follicular B		(68)
Plasma B		(68)
$CD4^+$ Helper T cell differentiation	0042093	
$CD4^+$ Helper T cell cytokine production	0035744, 0035745	
T cell extravasation	0072683	
CTL extravasation	0035697	
T cell chemotaxis	0010818	
CTL chemotaxis		(69)
CTL activity	0001916	
B cell proliferation	0042114	
Memory B cell differentiation		(70)
Plasma B cell differentiation	0002317	(71)
Follicular B cell differentiation	0002316	
+Effector T cell differentiation	0042492, 0045065	
+Naïve T cell proliferation	0033079	
+T helper subtypes activity	0072539, 0045063	
+B cell activation	0042113	
+B cell chemotaxis	0035754	

Table 1: Gene signatures were used to identify immune cell clusters, determine B and T cell subtypes, and perform pathway analysis. Gene signatures were collected from the Gene Ontology (GO) database. Certain pathways were supplemented with gene signatures identified in past literature. The pathways labeled with plus signs (+) did not show statistical significance and were not reported in our results.

database and relevant literature, we identified gene signatures for T cell chemotaxis, $CD4^+$ CTL and $CD8^+$ CTL chemotaxis, T cell extravasation, CTL extravasation, and $CD4^+$ CTL and $CD8^+$ CTL activity (**Table 1**). We then calculated the average gene expression of each pathway and compared the results across treatment groups.

We observed significantly higher expression of the T cell extravasation signature in the Kvax and combo treatment groups, compared to the control group (two-way ANOVA with Tukey HSD, $p < 0.0001$, $p < 0.0001$, respectively) **(Figure 6A)**. Further analysis of $CD8^+$ T cell extravasation revealed a significant elevation in the Kvax and CA170 treatment groups compared to the control group (two-way ANOVA with Tukey HSD, $p < 0.0001$, $p = 0.0266$, respectively), though no interaction was detected **(Figure 6B)**. T cell chemotaxis signatures exhibited significant increases in response to CA170 and Kvax individually compared to the control group (two-way ANOVA with Tukey HSD, $p < 0.0001$, $p < 0.0001$, respectively). This increase was further enhanced by the combo treatment as demonstrated by a significant interaction effect (two-way ANOVA with Tukey HSD, $p < 0.0001$) **(Figure 6C)**. Additionally, CTL infiltration, assessed via CTL chemotaxis, adhesion markers, and migration markers, was increased in the Kvax and combo treatment groups **(Figures 6D, E)**. These findings indicate the important role of Kvax in driving CTL infiltration. Furthermore, there was a strong expression of CTL activation-specific genes in the combo treatment group, confirming an increase in all CTL activity in the combo treatment group **(Figure 6F)**. These findings suggest that Kvax is the primary driver of increased gene expression related to T cell extravasation and T cell chemotaxis. Moreover, while CA170 or Kvax alone can enhance $CD8^+$ CTL chemotaxis and extravasation, they do not exhibit interaction in this process. Lastly, the combination of CA170 and Kvax enhanced CTL activity, whereas neither treatment alone did.

Effect of Treatment Groups on B Cell Compartments

Our proportion analysis revealed changes in B cell subtypes, while our receptor-ligand analysis revealed an upregulation of MHC interactions in the control group **(Figures 2E, 4C)**. To determine which B cell subtype was driving these changes, we examined B cell proliferation gene expression across subtypes. Memory B cells exhibited significantly higher expression of the proliferation pathway compared to follicular and plasma B cells (one-way ANOVA with Tukey HSD, $p < 0.01$, $p < 0.01$, respectively). This indicates that memory B cells may be more active in the lung TME **(Figure 7A)**. We then observed a significant increase in proliferation gene expression in response to CA170 and Kvax individually compared to the control group in memory B cells (two-way ANOVA; $p < 0.0001$, $p < 0.0001$, respectively) **(Figure 7B)**. Additionally, memory B cell differentiation gene expression was significantly enhanced by Kvax compared to the control group (two-way ANOVA with Tukey HSD, $p < 0.0001$) and a significant interaction effect was observed in the combo treatment (two-way ANOVA with Tukey HSD, $p = 0.0003$) **(Figure 7C)**. This suggests that Kvax alone or with CA170 drives an enhancement of memory B cell differentiation. In contrast, overall B cell proliferation was significantly reduced in the CA170 and combo treatment groups compared to the control group (two-way ANOVA with Tukey HSD, $p < 0.0001$, $p < 0.0001$, respectively) with a significant interaction effect ($p < 0.0001$) revealed by a two-way ANOVA. **(Figure 7D)**. Plasma B cell differentiation gene expression increased with Kvax treatment from the control group (two-way ANOVA with Tukey HSD, $p < 0.0001$) but decreased with CA170 and the combo treatment (two-way ANOVA with Tukey HSD, $p < 0.0001$, $p < 0.0001$, respectively) **(Figure 7E)**. Meanwhile, follicular B differentiation gene expression was significantly suppressed by Kvax ($p = 0.0026$) and the combo treatment ($p < 0.0001$) but increased by CA170 ($p < 0.0001$) compared to the control group, as reported by a two-way ANOVA followed by a Tukey HSD **(Figure 7F)**. These findings suggest that CA170 drives the decrease in overall B cell proliferation and plasma

https://doi.org/10.59720/24-358

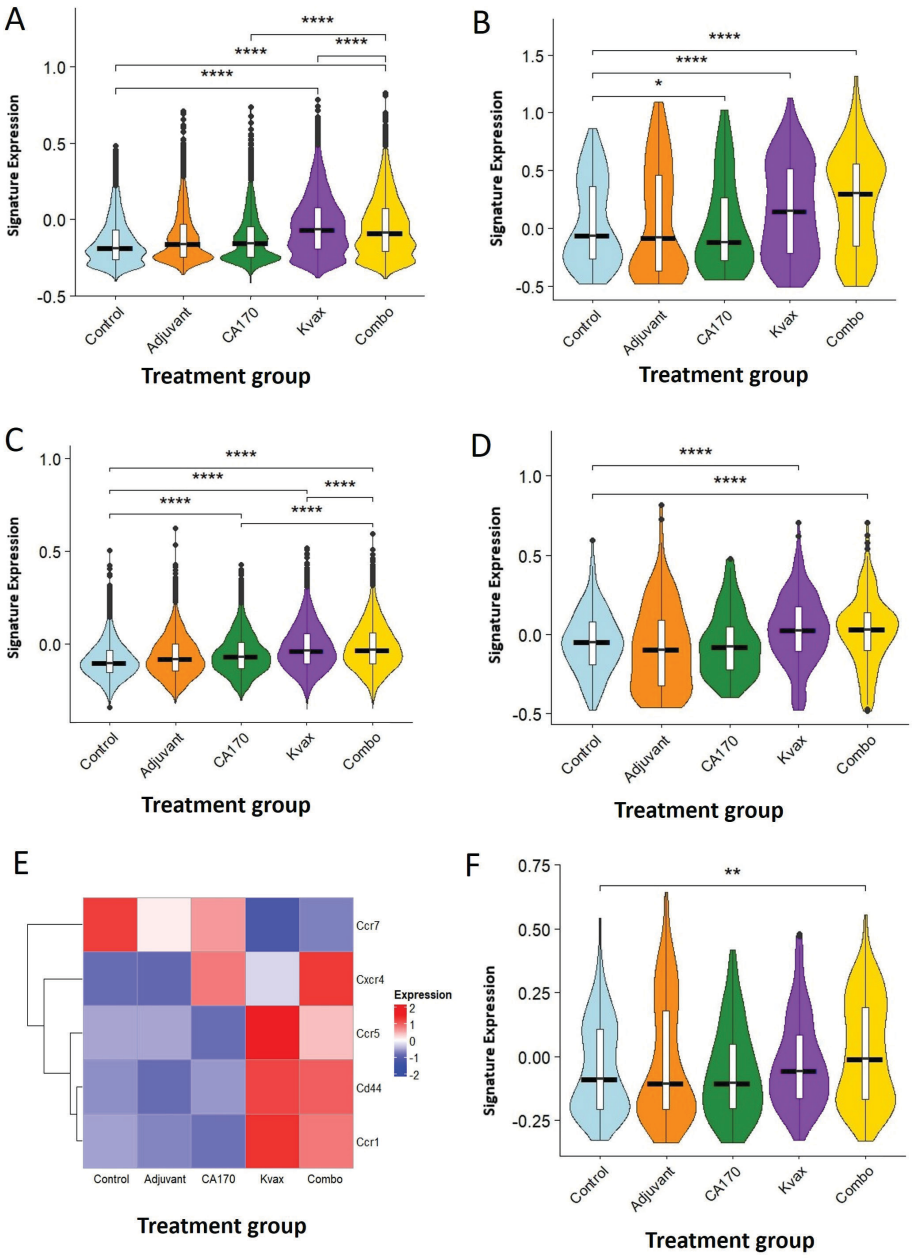

Figure 6: The Kvax and CA170/Kvax combination treatment groups induced cytotoxic T lymphocyte (CTL) and overall T cell migration. Average signature expression for each pathway and treatment group was calculated. The black lines on the violin plots represent median gene expression values. (A) Average T cell extravasation gene expression analyzed on T cells. The median values rounded to the thousandths place for each of the five treatment groups from left to right are as follows: control was -0.186, adjuvant was -0.158, CA170 was -0.153, KRAS vaccine (Kvax) was -0.064, combo was -0.085. Kvax had a significant difference on mean gene expression levels compared to the control group (two-way ANOVA with Tukey HSD, $p < 0.0001$). There was a significant interaction between CA170 and Kvax in influencing mean gene expression levels (two-way ANOVA with Tukey HSD, $p < 0.0001$). (B) Average $CD8^+$ CTL extravasation gene expression analyzed on $CD8^+$ CTLs. Median values: -0.059, -0.077, -0.114, 0.154, 0.305. CA170 and Kvax had a significant difference on mean gene expression levels compared to the control (two-way ANOVA with Tukey HSD, $p < 0.0266$, $p < 0.0001$). (C) Average T cell chemotaxis gene expression analyzed on T cells. Median values: -0.102, -0.082, -0.070, -0.036, -0.032. CA170 and Kvax had a significant difference on mean gene expression levels compared to the control (two-way ANOVA with Tukey HSD, $p < 0.0001$). The interaction between CA170 and Kvax was significant (two-way ANOVA with Tukey HSD, $p < 0.0001$). (D) Average CTL chemotaxis gene expression analyzed on both $CD8^+$ and $CD4^+$ CTLs. Median values: -0.048, -0.096, -0.076, 0.028, 0.032. Kvax had a significant difference on mean gene expression levels compared to the control (two-way ANOVA with Tukey HSD, $p < 0.0001$). (E) Heatmap showing average expression of cell adhesion and migration genes extracted from Figure 2B and analyzed on T cells. The dendrogram was clustered by hierarchical clustering. (F) Average CTL activation-specific gene expression analyzed on $CD8^+$ and $CD4^+$ CTLs. Median values: -0.088, -0.105, -0.103, -0.055, -0.008. The interaction between CA170 and Kvax was significant (two-way ANOVA with Tukey HSD, $p < 0.0049$). Two-way ANOVAs and Tukey post-hoc tests were performed on each pathway to examine the main effects of CA170 and Kvax and their interaction, * $p < 0.05$, ** $p < 0.01$, *** $p < 0.001$, **** $p < 0.0001$.

https://doi.org/10.59720/24-358

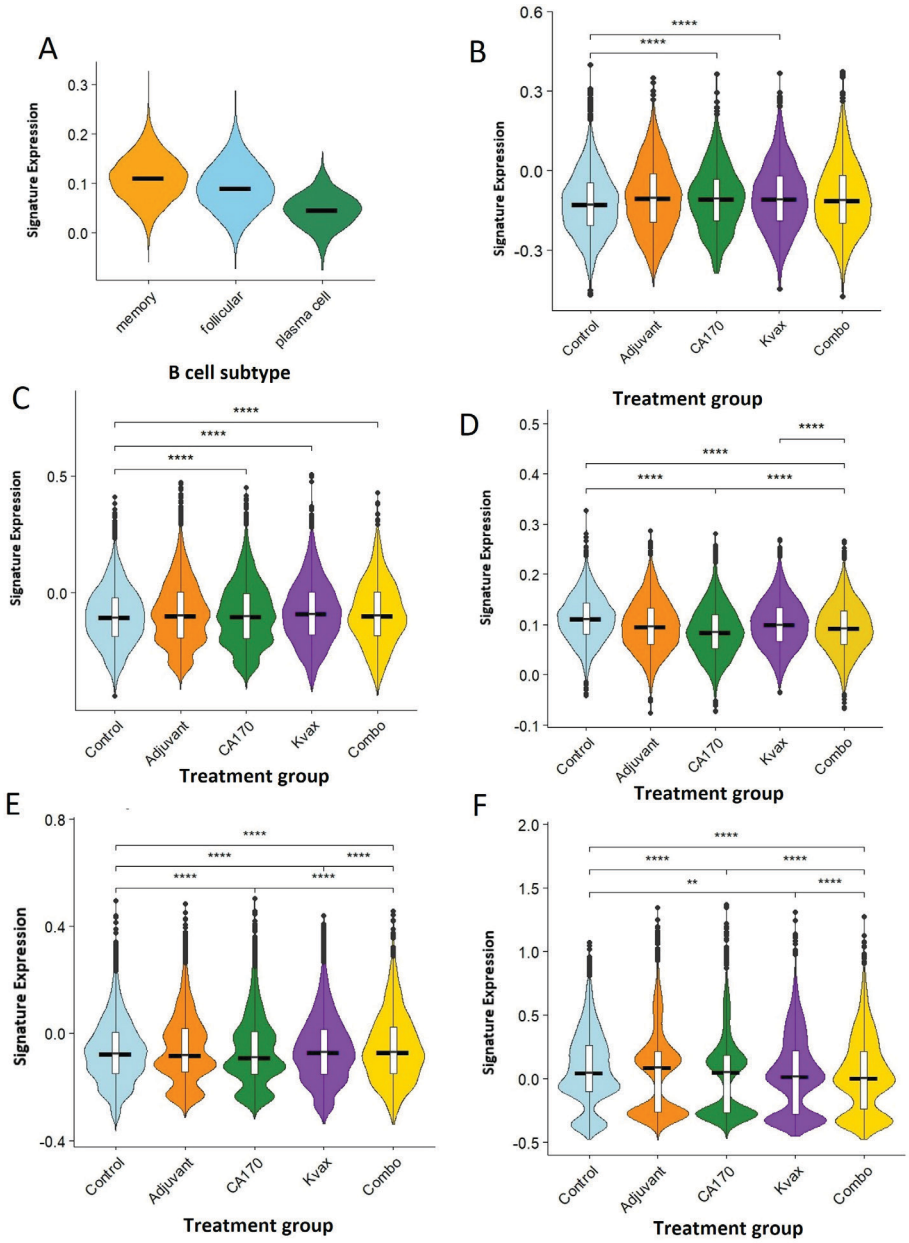

Figure 7: The interaction between Kvax and CA170 leads to an increase in memory B cells and plasma cells but an overall reduction in the proliferation of B cells. Average signature expression for each signature and treatment group was calculated. The black lines on the violin plots represent median gene expression values. (A) Average B cell proliferation gene expression across B cell subtypes. The median values rounded to the thousandths place for each of the three B cell subtypes from left to right are as follows: memory was 0.111, follicular was 0.091, plasma was 0.046. CA170 had a significant difference on mean gene expression levels compared to the control group (two-way ANOVA with Tukey HSD, $p < 0.0001$). There was a significant interaction between CA170 and KRAS vaccine (Kvax) in influencing mean gene expression levels (two-way ANOVA with Tukey HSD, $p < 0.0001$). (B) Average memory B cell proliferation gene expression analyzed on memory B cells. The median values rounded to the thousandths place for each of the treatment groups from left to right are as follows: control was -0.128, -0.103, -0.106, -0.108, -0.112. CA170 and Kvax had a significant difference on mean gene expression levels compared to the control (two-way ANOVA with Tukey HSD, $p < 0.0001$). (C) Average memory B cell differentiation gene expression analyzed on B cells. Median values: -0.103, -0.095, -0.099, -0.088, -0.095. Kvax had a significant difference on mean gene expression levels compared to the control (two-way ANOVA with Tukey HSD, $p < 0.0001$). The interaction between CA170 and Kvax was significant (two-way ANOVA with Tukey HSD, $p < 0.0003$). (D) Average B cell proliferation gene expression analyzed on B cells. Median values: 0.112, 0.096, 0.085, 0.100, 0.093. (E) Average plasma cell differentiation gene expression analyzed on B cells. Median values: 0.137, 0.137, 0.123, 0.144, 0.104. CA170 and Kvax had a significant difference on mean gene expression levels compared to the control (two-way ANOVA with Tukey HSD, $p < 0.0001$). The interaction between CA170 and Kvax was significant (two-way ANOVA with Tukey HSD, $p < 0.0001$). (F) Average follicular cell differentiation gene expression analyzed on B cells. Median values: 0.048, 0.087, 0.051, 0.016. CA170 and Kvax had a significant difference on mean gene expression levels compared to the control (two-way ANOVA with Tukey HSD, $p < 0.0001$, $p = 0.0026$). The interaction between CA170 and Kvax was significant (two-way ANOVA with Tukey HSD, $p < 0.0001$). Two-way ANOVAs and Tukey post-hoc tests were performed on each pathway to examine the main effects of CA170 and Kvax and their interaction, ** $p < 0.01$, **** $p < 0.0001$.

https://doi.org/10.59720/24-358

B cell differentiation, while Kvax is responsible for repressing follicular B cell differentiation and promoting memory B cell differentiation. Despite decreases in other B cell subtype activity, both treatments enhance memory B cell function.

DISCUSSION

In recent years, the emergence of ICIs has driven advancements in lung cancer treatment. However, the efficacy of existing ICIs varies, and drug resistance remains a challenge, underscoring the need for novel ICI targets (18). VISTA, known for its strong suppression of T cell functions and abundant expression in lung tissue, presents an excellent target for ICI inhibitors (24). While mAbs can target VISTA, their large molecular size limits tumor tissue infiltration (44). In contrast, small-molecule antagonist ICI CA170 demonstrates distinct advantages by inhibiting multiple immune checkpoints simultaneously (17). Its small size allows for efficient tumor infiltration, enhancing immune checkpoint suppression (20, 24, 45).

In addition to CA170, we also investigated the impact of Kvax on immune cell populations. Kvax was designed to target *KRAS* mutations, a main driver of lung cancer (46). Our findings support our hypothesis that CA170 combined with Kvax enhances the antitumor response more than either treatment alone. Using scRNA-seq data analysis, we found that the combination of CA170 and Kvax amplifies immune cell response pathways in a more effective manner than ICI treatment alone. Specifically, we observed increased helper T cell proliferation and activity, enhanced T cell migration, reduced overall B cell proliferation, and increased memory B and plasma cell proliferation in the combo treatment group.

Our scRNA-seq analysis utilized data samples previously collected by Pan et al (23). While their study employed flow cytometry and *in vivo* experiments to identify increased T cell infiltration and helper T cell numbers, our study further explores the cellular pathways involved with these processes and provides a more detailed characterization of T cell subtypes. Notably, our analysis also offers novel insight into B cell subtype proliferation and differentiation within the lung TME. The scRNA-seq analysis and cell subtype identification are slightly different between Pan et al.'s study and our study due to varying quality control thresholds and clustering criteria (number of genes detected per cell, percent mitochondrial genes, number of principal components, UMAP vs tSNE).

Naive $CD4^+$ T cells differentiate into effector, memory, and helper T lymphocytes when exposed to antigens, costimulatory molecules, and cytokines in the TME (47). By producing cytokines that regulate CTL activity and inhibit tumor blood vessel formation, helper T cells play a key role in antitumor responses (48). Higher levels of total helper T cells are associated with improved immune-mediated tumor control and survival rates (49). When CA170 was combined with Kvax, the proportion of helper T cells expanded, aligning with the increased expression of helper T cell gene markers in T cells **(Figures 2D, 3B)**. This trend was consistent with the observed upregulation of helper T cell differentiation and function following CA170 and Kvax treatments **(Figures 5A, B, C)**. Furthermore, the combo treatment group demonstrated markedly higher expression of helper T cell functional pathways compared to the Kvax and CA170 groups alone **(Figures 5A, B, C)**. This finding suggests an interactive effect between CA170 and Kvax that enhances helper T cell numbers and functions, ultimately improving the antitumor response. Given the observed increase in helper T cell activity, future studies could explore the interactions of specific helper T cell subsets (i.e., Th1, Th17, Th2) in response to CA170 and Kvax.

T cell infiltration is associated with improved antitumor response and survival outcomes (43). CTLs play a key role in T cell migration and attack by identifying and killing tumor cells, releasing chemokines, and recruiting additional CTLs (50). A closely related process to chemotaxis is extravasation, in which cells exit blood vessels and migrate into tissues (51). Our analysis of T cell migration revealed a marked increase in T cell extravasation gene expressions in response to Kvax, CA170, and the combo treatment **(Figure 6A)**. Similarly, T cell chemotaxis gene expressions increased in the Kvax and combo treatment groups **(Figure 6C)**. We observed that CTL, including both $CD8^+$ and $CD4^+$ CTL, chemotaxis and extravasation were primarily driven by Kvax, though no interaction with CA170 was observed **(Figures 6B, D)**. This increase was consistent with enhanced CTL activity and higher expression of CTL adhesion and migration genes in the Kvax and combo treatment groups compared to the control **(Figures 6E, F)**. These findings suggest that Kvax, alone or combined with CA170, promotes CTL migration towards and infiltration into the tumor, enhancing the immune response. Prior studies also support Kvax's role in increasing $CD8^+$ CTL infiltration into tumors (52).

While most studies on immune response following ICI treatments have focused on T lymphocytes, changes in B lymphocytes remain underexplored (11, 12, 53, 54). The composition of the B cell compartment plays a key role in antitumor responses and subsequent diseases. B cells can facilitate T cell responses by presenting antigens, ultimately inhibiting tumor growth (55). Additionally, B cells can form tertiary lymphoid structures in tumors, consisting of follicular and plasma B cells, to increase B cell presence in the tumor, produce antibodies, and present antigens (56). However, regulatory B cells can release anti-inflammatory cytokines to induce regulatory T cells and myeloid-derived immunosuppressive cells, limiting the antitumor immune response (56). Understanding these B cell responses to ICIs and cancer vaccines could contribute to more effective immunotherapies that incorporate B cell antitumor effects or prevent B cell pro-tumor effects.

Our results suggested that the B cell compartments were remodeled in response to CA170, Kvax, and the combo treatment group **(Figures 2E, F, 3C, E, F).** Interestingly, memory B cell proportions as well as memory B cell marker gene expression were highest in the control group **(Figures 2E, 3C)**. Additionally, overall B cell and follicular B cell proliferation decreased in response to the combo treatment **(Figures 7D, F)**. Meanwhile, memory B and plasma cell proliferation increased with the Kvax treatment **(Figures 7B, E)**. These findings align with previous research, which showed that treatment of a combined checkpoint blockade reduced total circulating B cells while enriching plasmablasts and proliferative memory B cells (57, 58).

This study represents the first analysis of B-cell signaling pathways in response to the *KRAS* vaccine or VISTA ICI

https://doi.org/10.59720/24-358

therapy. The observed changes in B cell subtype differentiation could be attributed to the *KRAS* antigen vaccine. Antigen vaccines are known to activate antigen-presenting cells, including B cells, to initiate and amplify a T cell response. These activated B cells typically differentiate into memory germinal center B cells and antibody-producing plasma B cells (28). While specific antigen-presenting cells involved in the Kvax response have not been well-studied, our observed increase in memory and plasma B cell differentiation in the Kvax group aligns with the expected effect of other antigen vaccines (59). This suggests that B cells play a key role in presenting the *KRAS* antigens. Given their importance in antitumor immunity, further investigation into B cell pathways in response to cancer antigen vaccines is warranted. The data used in our study was collected from carcinogen-induced primary murine lung tumor models. While these murine tumor models resemble human lung cancer in molecular morphology and histopathology, using human lung cancer cell data would ensure greater relevance to human biology, improve the translational potential of our findings, and reduce species-specific differences that could impact results.

Additionally, our B cell-related findings were based on scRNA-seq data and should be validated through laboratory experiments, such as flow cytometry to assess proportion changes, co-culturing B and T cells with Kvax to observe B cell antigen presentation, and tissue staining to visualize the *in vivo* immune landscape. Future studies should further investigate the underlying molecular interactions with B cells and their physiological significance. Notably, we observed strong receptor-ligand interactions between Natural Killer T (NKT) cells and both B and T cells **(Figure 4A)**. Since NKT cells recognize cancer cells and rapidly produce cytokines to regulate other immune cells in the TME, they represent a promising target for cancer immunotherapies (60). Given that NKT cell proportions in the control group were nearly four times higher than in the Kvax-treated group **(Figure 2A)**, further research should explore their role in cancer vaccines and combination therapies. Finally, future studies could examine the therapeutic potential of combining antigen-specific vaccines with ICIs in other cancers (61, 62).

In summary, our findings suggest that the immune checkpoint inhibitor CA170, in combination with the antigen-specific vaccine Kvax, may improve antitumor efficacy in treating lung cancer. The success of this combination therapy could inform new strategies to improve immunotherapy outcomes for lung cancer patients. Furthermore, our novel findings on a VISTA inhibitor's effect on B cell populations and activity highlight a potential new avenue for immunotherapy development and deepen our understanding of diverse immune response pathways.

MATERIALS AND METHODS

Dataset

Gene-level scRNA-seq data from primary murine lung cancer samples collected by Pan et al. were downloaded from the GEO with accession number GSE176091 (23, 30). The dataset consisted of 20 samples collected from mouse models that developed carcinogen-induced lung adenomas and adenocarcinomas, mirroring key characteristics of human lung tumors. These murine lung tumors were induced by vinyl-carbamate injections, a compound known to drive *KRAS* mutations. The samples were divided into five treatment groups: 1) control mice administered phosphate-buffered saline, 2) adjuvant control mice treated with a STING agonist, 3) Kvax mice treated with an MHCII-directed *KRAS* peptide vaccine plus adjuvant, 4) CA170 mice treated with CA170, and 5) combo mice treated with a combination of CA170, Kvax, and adjuvant. Data analysis was performed across these groups to evaluate treatment effects on gene expressions (30).

Single-cell RNA Sequencing Data Processing

Data were analyzed in R (version 4.4.0) using Seurat (version 5.1.0) (31, 32). To ensure data quality, doublets, droplets, and dead cells were removed using the following criteria: cells expressing fewer than 200 genes or more than 5000 genes, and cells with more than 10% mitochondrial genes. After filtering, the number of analyzed cells per group was as follows: 14,540 cells for the control group, 14,587 cells for the adjuvant group, 14,821 cells for the CA170 treatment group, 16,575 cells for the Kvax treatment group, and 16,733 cells for the combo treatment group. Gene expression data from the $CD45^+$ object were log-normalized and scaled on all cells across all treatment groups using the NormalizeData() and scale() functions in R. The scaling function centered each gene's expression by subtracting its mean and dividing by its standard deviation. Subsequently, principal component analysis (PCA) was conducted. The five most statistically significant principal components were used to generate a uniform manifold approximation and projection (UMAP) visualization.

Clusters Identification

Within the $CD45^+$ object, we clustered cells using the FindAllMarkers() function, considering only genes expressed in more than 25% of cells with at least a 0.25-fold difference. Then, we identified B cells, T cells, neutrophils, myeloid cells, NK cells, NKT cells, and dendritic cells based on common gene markers **(Figure 1A)** (63-66). T cells were identified based on high expression of *Cd3*, *Cd4*, and *Cd8* genes, while B cells were identified based on elevated expression of *Bank1* and *Cd79a* genes. Subtypes within the B and T cell clusters were identified using key gene signatures **(Figures 1B, C)** (67, 68).

Pathway Analysis

To analyze immune cell response pathways, we conducted receptor-ligand analysis via CellChat (version 1.6.1), an R package designed to infer cellular communication pathways. Gene signatures from the GO database were used to investigate immune pathways **(72, 73)**. For pathways containing fewer than four genes in the GO database, key gene signatures were obtained from previous studies. Some of the genes from the GO database were not expressed in the data samples. Therefore, they were not included in the analysis. Once the signature genes were identified, the AddModuleScore function in Seurat was used to calculate the average gene expression of each signature. AddModuleScore calculates an average expression score for a specified list of genes and then subtracts the average expression of randomly

https://doi.org/10.59720/24-358

selected control genes to account for overall expression levels. The resulting average gene expressions were tested for statistical significance across treatments.

The full programming script for data processing and analysis is accessible on GitHub in the following repository: https://github.com/chloegig/scRNA-seq-analysis.

Statistics

One-way ANOVA tests and Tukey HSD post-hoc tests were performed using the Vassar Stats computational tool to evaluate the significance of B cell proliferation gene expression across B cell subtypes (74). All other pathway analyses were tested for significance with the Vassar Stats two-way ANOVA test and Tukey HSD post-hoc test since they were compared across treatment groups. The two-way ANOVA design included the presence of CA170 as one factor and the presence of Kvax as the other. The control group, rather than the adjuvant group, was used as the baseline without either treatment. Statistical significance was defined as $p < 0.05$ (*), $p < 0.01$ (**), $p < 0.001$ (***), and $p < 0.0001$ (****).

Received: September 9, 2024
Accepted: March 14, 2025
Published: March 16, 2026

REFERENCES

1. Wang, B. et al. "Effective Antitumor Immunity Can Be Triggered by Targeting Vista in Combination with a Tlr3-Specific Adjuvant." *Cancer Immunol Res*, vol. 11, no. 12, 2023, pp. 1656-70, https://doi.org/10.1158/2326-6066.CIR-23-0117.
2. "Key Statistics for Lung Cancer | How Common Is Lung Cancer?" *American Cancer Society.* https://www.cancer.org/cancer/types/lung-cancer/about/key-statistics.html. Accessed 7 Jun. 2025.
3. Bi, J. H. et al. "Observed and Relative Survival Trends of Lung Cancer: A Systematic Review of Population-Based Cancer Registration Data." *Thorac Cancer*, vol. 15, no. 2, 2024, pp. 142-51, https://doi.org/10.1111/1759-7714.15170.
4. Yu, L. et al. "[Prognosis Analysis of Early-Stage Non-Small Cell Lung Cancer Patients Treated with Stereotactic Body Radiotherapy]." *Zhongguo Fei Ai Za Zhi*, vol. 26, no. 4, 2023, pp. 274-80, https://doi.org/10.3779/j.issn.1009-3419.2023.102.13.
5. *State of Lung Cancer 2020 Report*. American Lung Association, 2020.
6. Guo, Q. et al. "Current Treatments for Non-Small Cell Lung Cancer." *Front Oncol*, vol. 12, 2022, p. 945102, https://doi.org/10.3389/fonc.2022.945102.
7. Anderson, Nicole M., and M. Celeste Simon. "The Tumor Microenvironment." Current Biology, vol. 30, no. 16, Aug. 2020, pp. R921–R925, https://doi.org/10.1016/j.cub.2020.06.081.
8. Delves, Peter J., and Ivan M. Roitt. "The Immune System." New England Journal of Medicine, vol. 343, no. 1, 6 July 2000, pp. 37–49, https://doi.org/10.1056/nejm200007063430107.
9. Loose, David, and Christophe Van de Wiele. "The Immune System and Cancer." *Cancer Biotherapy and Radiopharmaceuticals*, vol. 24, no. 3, June 2009, pp. 369–376, https://doi.org/10.1089/cbr.2008.0593.
10. Pardoll, D. M. "The Blockade of Immune Checkpoints in Cancer Immunotherapy." *Nat Rev Cancer*, vol. 12, no. 4, 2012, pp. 252-64, https://doi.org/10.1038/nrc3239.
11. Granier, C. et al. "Mechanisms of Action and Rationale for the Use of Checkpoint Inhibitors in Cancer." *ESMO Open*, vol. 2, no. 2, 2017, p. e000213, https://doi.org/10.1136/esmoopen-2017-000213.
12. Reck, M. et al. "Pembrolizumab Versus Chemotherapy for Pd-L1-Positive Non-Small-Cell Lung Cancer." *N Engl J Med*, vol. 375, no. 19, 2016, pp. 1823-33, https://doi.org/10.1056/NEJMoa1606774.
13. Topalian, S. L. et al. "Immune Checkpoint Blockade: A Common Denominator Approach to Cancer Therapy." *Cancer Cell*, vol. 27, no. 4, 2015, pp. 450-61, https://doi.org/10.1016/j.ccell.2015.03.001.
14. Shah, Kinjal, et al. "T Cell Receptor (TCR) Signaling in Health and Disease." *Signal Transduction and Targeted Therapy*, vol. 6, no. 1, 13 Dec. 2021, pp. 1–26, https://doi.org/10.1038/s41392-021-00823-w.
15. Lynch, T. J. et al. "Ipilimumab in Combination with Paclitaxel and Carboplatin as First-Line Treatment in Stage Iiib/Iv Non-Small-Cell Lung Cancer: Results from a Randomized, Double-Blind, Multicenter Phase II Study." *J Clin Oncol*, vol. 30, no. 17, 2012, pp. 2046-54, https://doi.org/10.1200/JCO.2011.38.4032.
16. Philips, G. K. and M. Atkins. "Therapeutic Uses of Anti-Pd-1 and Anti-Pd-L1 Antibodies." *Int Immunol*, vol. 27, no. 1, 2015, pp. 39-46, https://doi.org/10.1093/intimm/dxu095.
17. Chen, L. et al. "Development of Small Molecule Drugs Targeting Immune Checkpoints." *Cancer Biol Med*, vol. 21, no. 5, 2024, pp. 382-99, https://doi.org/10.20892/j.issn.2095-3941.2024.0034.
18. Hwang, S. et al. "Immune Gene Signatures for Predicting Durable Clinical Benefit of Anti-Pd-1 Immunotherapy in Patients with Non-Small Cell Lung Cancer." *Sci Rep*, vol. 10, no. 1, 2020, p. 643, https://doi.org/10.1038/s41598-019-57218-9.
19. Chen, S. et al. "Small-Molecule Immuno-Oncology Therapy: Advances, Challenges and New Directions." *Curr Top Med Chem*, vol. 19, no. 3, 2019, pp. 180-85, https://doi.org/10.2174/1568026619666190308131805.
20. Sasikumar, P. G. et al. "Pd-1 Derived Ca-170 Is an Oral Immune Checkpoint Inhibitor That Exhibits Preclinical Anti-Tumor Efficacy." *Commun Biol*, vol. 4, no. 1, 2021, p. 699, https://doi.org/10.1038/s42003-021-02191-1.
21. Xu, Wenwen, et al. "The Structure, Expression, and Multifaceted Role of Immune-Checkpoint Protein VISTA as a Critical Regulator of Anti-Tumor Immunity, Autoimmunity, and Inflammation." *Cellular & Molecular Immunology*, vol. 15, no. 5, 1 May 2018, pp. 438–446, https://doi.org/10.1038/cmi.2017.148.
22. Franz Villarroel-Espindola, et al. Spatially Resolved and Quantitative Analysis of VISTA/PD-1H as a Novel Immunotherapy Target in Human Non–Small Cell Lung Cancer. Vol. 24, no. 7, 1 Apr. 2018, pp. 1562–1573, https://doi.org/10.1158/1078-0432.CCR-17-2542.

https://doi.org/10.59720/24-358

23. Pan, J. et al. "Inhibition of Lung Tumorigenesis by a Small Molecule Ca170 Targeting the Immune Checkpoint Protein Vista." *Commun Biol*, vol. 4, no. 1, 2021, p. 906, https://doi.org/10.1038/s42003-021-02381-x.
24. Lines, J. L. et al. "Vista Is an Immune Checkpoint Molecule for Human T Cells." *Cancer Res*, vol. 74, no. 7, 2014, pp. 1924-32, https://doi.org/10.1158/0008-5472.CAN-13-1504.
25. Kiat, Tony, et al. "KRAS G12C in Advanced NSCLC: Prevalence, Co-Mutations, and Testing." *Lung Cancer*, vol. 184, 1 Oct. 2023, pp. 107293–107293, https://doi.org/10.1016/j.lungcan.2023.107293.
26. Massey, T. E. et al. "High Frequency of K-Ras Mutations in Spontaneous and Vinyl Carbamate-Induced Lung Tumors of Relatively Resistant B6cf1 (C57bl/6j X Balb/Cj) Mice." *Carcinogenesis*, vol. 16, no. 5, 1995, pp. 1065-9, https://doi.org/10.1093/carcin/16.5.1065.
27. Kleponis, Jennifer, et al. "Fueling the Engine and Releasing the Break: Combinational Therapy of Cancer Vaccines and Immune Checkpoint Inhibitors." *Cancer Biology & Medicine*, vol. 12, no. 3, 1 Sept. 2015, pp. 201–208, https://doi.org/10.7497/j.issn.2095-3941.2015.0046.
28. Hinke, Daniëla Maria, et al. "Antigen Bivalency of Antigen-Presenting Cell-Targeted Vaccines Increases B Cell Responses." *Cell Reports*, vol. 39, no. 9, 1 May 2022, pp. 110901–110901, https://doi.org/10.1016/j.celrep.2022.110901.
29. Zhao, Y. et al. "Single-Cell Transcriptomics of Immune Cells Reveal Diversity and Exhaustion Signatures in Non-Small-Cell Lung Cancer." *Front Immunol*, vol. 13, 2022, p. 854724, https://doi.org/10.3389/fimmu.2022.854724.
30. "Geo Accession Viewer." *National Institute of Health*. ncbi.nlm.nih.gov/geo/query/acc.cgi?acc=GSE176091. Accessed 20 Jun. 2024.
31. R Core Team. *R: A Language and Environment for Statistical Computing*. Version 4.4.0, R Foundation for Statistical Computing, 2024, https://www.r-project.org/. Accessed 7 Jun. 2025.
32. Satija Lab. *Seurat: Tools for Single Cell Genomics*. Version 5.1.0, Satija Lab, 2024, satijalab.org/seurat/. Accessed 7 Jun. 2025.
33. Wang, Bin, et al. "Clinical Applications of STING Agonists in Cancer Immunotherapy: Current Progress and Future Prospects." Frontiers in Immunology, vol. 15, 2 Oct. 2024, https://doi.org/10.3389/fimmu.2024.1485546.
34. Jin, Suoqin, et al. "Inference and Analysis of Cell-Cell Communication Using CellChat." *Nature Communications*, vol. 12, no. 1, 17 Feb. 2021, https://doi.org/10.1038/s41467-021-21246-9.
35. Ponta, H. et al. "Cd44: From Adhesion Molecules to Signalling Regulators." *Nat Rev Mol Cell Biol*, vol. 4, no. 1, 2003, pp. 33-45, https://doi.org/10.1038/nrm1004.
36. Ottoson, N. C. et al. "Cutting Edge: T Cell Migration Regulated by Cxcr4 Chemokine Receptor Signaling to Zap-70 Tyrosine Kinase." *J Immunol*, vol. 167, no. 4, 2001, pp. 1857-61, https://doi.org/10.4049/jimmunol.167.4.1857.
37. Weber, C. et al. "Specialized Roles of the Chemokine Receptors Ccr1 and Ccr5 in the Recruitment of Monocytes and T(H)1-Like/Cd45ro(+) T Cells." *Blood*, vol. 97, no. 4, 2001, pp. 1144-6, https://doi.org/10.1182/blood.v97.4.1144.
38. Ugolini, S. and E. Vivier. "Multifaceted Roles of Mhc Class I and Mhc Class I-Like Molecules in T Cell Activation." *Nat Immunol*, vol. 2, no. 3, 2001, pp. 198-200, https://doi.org/10.1038/85246.
39. Ohtsuka, M. et al. "Major Histocompatibility Complex (Mhc) Class Ib Gene Duplications, Organization and Expression Patterns in Mouse Strain C57bl/6." *BMC Genomics*, vol. 9, 2008, p. 178, https://doi.org/10.1186/1471-2164-9-178.
40. Li, Y. et al. "Structural and Biophysical Insights into the Role of Cd4 and Cd8 in T Cell Activation." *Front Immunol*, vol. 4, 2013, p. 206, https://doi.org/10.3389/fimmu.2013.00206.
41. "Molecular Function Gene Ontology Term (Go:0003674)." *JAX*. informatics.jax.org/vocab/gene_ontology. Accessed 23 Jul. 2024.
42. Yang, W. et al. "T-Cell Infiltration and Its Regulatory Mechanisms in Cancers: Insights at Single-Cell Resolution." *J Exp Clin Cancer Res*, vol. 43, no. 1, 2024, p. 38, https://doi.org/10.1186/s13046-024-02960-w.
43. Slaney, C. Y. et al. "Trafficking of T Cells into Tumors." *Cancer Res*, vol. 74, no. 24, 2014, pp. 7168-74, https://doi.org/10.1158/0008-5472.CAN-14-2458.
44. Dahan, R. et al. "Fcgammars Modulate the Anti-Tumor Activity of Antibodies Targeting the Pd-1/Pd-L1 Axis." *Cancer Cell*, vol. 28, no. 3, 2015, pp. 285-95, https://doi.org/10.1016/j.ccell.2015.08.004.
45. Wang, F. et al. "Small-Molecule Agents for Cancer Immunotherapy." *Acta Pharm Sin B*, vol. 14, no. 3, 2024, pp. 905-52, https://doi.org/10.1016/j.apsb.2023.12.010.
46. Pan, J. et al. "Immunoprevention of Kras-Driven Lung Adenocarcinoma by a Multipeptide Vaccine." *Oncotarget*, vol. 8, no. 47, 2017, pp. 82689-99, https://doi.org/10.18632/oncotarget.19831.
47. Zhu, J. et al. "Differentiation of Effector CD4 T Cell Populations*." *Annu Rev Immunol*, vol. 28, 2010, pp. 445-89, https://doi.org/10.1146/annurev-immunol-030409-101212.
48. Xie, L. et al. "The Role of $Cd4^+$ T Cells in Tumor and Chronic Viral Immune Responses." *MedComm (2020)*, vol. 4, no. 5, 2023, p. e390, https://doi.org/10.1002/mco2.390.
49. Yang, X. et al. "Peripheral $CD4^+$ T Cells Correlate with Response and Survival in Patients with Advanced Non-Small Cell Lung Cancer Receiving Chemo-Immunotherapy." *Front Immunol*, vol. 15, 2024, p. 1364507, https://doi.org/10.3389/fimmu.2024.1364507.
50. Harlin, H. et al. "Chemokine Expression in Melanoma Metastases Associated with $CD8^+$ T-Cell Recruitment." *Cancer Res*, vol. 69, no. 7, 2009, pp. 3077-85, https://doi.org/10.1158/0008-5472.CAN-08-2281.
51. Strell, C. and F. Entschladen. "Extravasation of Leukocytes in Comparison to Tumor Cells." *Cell Commun Signal*, vol. 6, 2008, p. 10, https://doi.org/10.1186/1478-811X-6-10.
52. Pan, J. et al. "Potentiation of Kras Peptide Cancer Vaccine by Avasimibe, a Cholesterol Modulator." *EBioMedicine*, vol. 49, 2019, pp. 72-81, https://doi.org/10.1016/j.ebiom.2019.10.044.

https://doi.org/10.59720/24-358

53. Sharma, Padmanee, and James P Allison. “Immune Checkpoint Targeting in Cancer Therapy: Toward Combination Strategies with Curative Potential.” *Cell*, vol. 161, no. 2, 2015, pp. 205–14, https://doi.org/10.1016/j.cell.2015.03.030.
54. Ribas, Antoni. “Releasing the Brakes on Cancer Immunotherapy.” *New England Journal of Medicine*, vol. 373, no. 16, 15 Oct. 2015, pp. 1490–1492, https://doi.org/10.1056/NEJMp1510079.
55. Sarvaria, Anushruti, et al. “B Cell Regulation in Cancer and Anti-Tumor Immunity.” *Cellular & Molecular Immunology*, vol. 14, no. 8, 19 June 2017, pp. 662–674, www.ncbi.nlm.nih.gov/pmc/articles/PMC5549607/, https://doi.org/10.1038/cmi.2017.35.
56. Esparcia-Pinedo, Laura, et al. “Tertiary Lymphoid Structures and B Lymphocytes: A Promising Therapeutic Strategy to Fight Cancer.” *Frontiers in Immunology*, vol. 14, 9 Aug. 2023, https://doi.org/10.3389/fimmu.2023.1231315.
57. Das, R. et al. "Early B Cell Changes Predict Autoimmunity Following Combination Immune Checkpoint Blockade." *J Clin Invest*, vol. 128, no. 2, 2018, pp. 715-20, https://doi.org/10.1172/JCI96798.
58. Kuehn, H. S. et al. "Immune Dysregulation in Human Subjects with Heterozygous Germline Mutations in Ctla4." *Science*, vol. 345, no. 6204, 2014, pp. 1623-27, https://doi.org/10.1126/science.1255904.
59. “NCI Drug Dictionary.” *Cancer.gov*, 2025, https://www.cancer.gov/publications/dictionaries/cancer-drug/def/mrna-derived-kras-targeted-vaccine-v941. Accessed 7 Jun. 2025.
60. Nelson, Adam, et al. “The Current Landscape of NKT Cell Immunotherapy and the Hills Ahead.” *Cancers*, vol. 13, no. 20, 15 Oct. 2021, p. 5174, https://doi.org/10.3390/cancers13205174.
61. Kleponis, J. et al. "Fueling the Engine and Releasing the Break: Combinational Therapy of Cancer Vaccines and Immune Checkpoint Inhibitors." *Cancer Biol Med*, vol. 12, no. 3, 2015, pp. 201-8, https://doi.org/10.7497/j.issn.2095-3941.2015.0046.
62. Fan, T. et al. "Therapeutic Cancer Vaccines: Advancements, Challenges, and Prospects." *Signal Transduct Target Ther*, vol. 8, no. 1, 2023, p. 450, https://doi.org/10.1038/s41392-023-01674-3.
63. Hackert, Nicolaj S., et al. “Human and Mouse Neutrophils Share Core Transcriptional Programs in Both Homeostatic and Inflamed Contexts.” *Nature Communications*, vol. 14, no. 1, 8 Dec. 2023, p. 8133, https://doi.org/10.1038/s41467-023-43573-9.
64. Zheng, Su-Su, et al. “A Novel Myeloid Cell Marker Genes Related Signature Can Indicate Immune Infiltration and Predict Prognosis of Hepatocellular Carcinoma: Integrated Analysis of Bulk and Single-Cell RNA Sequencing.” *Frontiers in Molecular Biosciences*, vol. 10, July 2023, p. 1118377, https://doi.or/10.3389/fmolb.2023.1118377.
65. McFarland, Adelle P, et al. *Multi-Tissue Single-Cell Analysis Deconstructs the Complex Programs of Mouse Natural Killer and Type 1 Innate Lymphoid Cells in Tissues and Circulation*. Vol. 54, no. 6, 1 June 2021, pp. 1320-1337.e4, https://doi.org/10.1016/j.immuni.2021.03.024.
66. Hongo, David, et al. “Identification of Two Subsets of Murine DC1 Dendritic Cells That Differ by Surface Phenotype, Gene Expression, and Function.” *Frontiers in Immunology*, vol. 12, 2021, p. 746469, https://doi.org/10.3389/fimmu.2021.746469.
67. Mullan, K. A. et al. "Current Annotation Strategies for T Cell Phenotyping of Single-Cell Rna-Seq Data." *Front Immunol*, vol. 14, 2023, p. 1306169, https://doi.org/10.3389/fimmu.2023.1306169.
68. "B Cells." *Bio-Techne*. https://www.rndsystems.com/resources/cell-markers/immune-cells/b-cells. Accessed 7 Jun. 2025.
69. Jung, Steffen, et al. “In Vivo Depletion of CD11c+ Dendritic Cells Abrogates Priming of CD8+ T Cells by Exogenous Cell-Associated Antigens.” Immunity, vol. 17, no. 2, Aug. 2002, pp. 211–220, https://doi.org/10.1016/s1074-7613(02)00365-5.
70. Anderson, Shannon M., et al. “New Markers for Murine Memory B Cells That Define Mutated and Unmutated Subsets.” Journal of Experimental Medicine, vol. 204, no. 9, 13 Aug. 2007, pp. 2103–2114, https://doi.org/10.1084/jem.20062571.
71. Grasseau, Alexis, et al. “The Diversity of the Plasmablast Signature across Species and Experimental Conditions: A Meta-Analysis.” Immunology, vol. 164, no. 1, 26 May 2021, pp. 120–134, https://doi.org/10.1111/imm.13344.
72. Ashburner, Michael, et al. “Gene Ontology: Tool for the Unification of Biology.” Nature Genetics, vol. 25, no. 1, May 2000, pp. 25–29, https://doi.org/10.1038/75556.
73. Aleksander, Suzi, et al. “The Gene Ontology Knowledgebase in 2023.” Genetics, vol. 224, no. 1, 3 Mar. 2023, https://doi.org/10.1093/genetics/iyad031.
74. Lowry, Richard. *VassarStats: Website for Statistical Computation*. vassarstats.net/. Accessed 18 May 2025.